High glucose treatment promotes extracellular matrix proteome remodeling in Müller glial cells

Sandra Sagmeister [1, 2], **Juliane Merl-Pham** [2], **Agnese Petrera** [2], **Cornelia A Deeg** [Corresp., 1], **Stefanie M Hauck** [Corresp. 2]

[1] Chair of Physiology, Department of Veterinary Sciences, LMU Munich, Martinsried, Germany

[2] Research Unit Protein Science and Metabolomics and Proteomics Core Facility, Helmholtz Center Munich, German Research Center for Environmental Health GmbH, Munich, Germany

Corresponding Authors: Cornelia A Deeg, Stefanie M Hauck
Email address: Cornelia.Deeg@lmu.de, hauck@helmholtz-muenchen.de

Background. The underlying pathomechanisms in diabetic retinopathy (DR) remain incompletely understood. The aim of this study was to add to the current knowledge about the particular role of retinal Müller glial cells (RMG) in the initial processes of DR. **Methods.** Applying a quantitative proteomic workflow, we investigated changes of primary porcine RMG under short term high glucose treatment as well as glycolysis inhibition treatment. **Results.** We revealed significant changes in RMG proteome primarily in proteins building the extracellular matrix (ECM) indicating fundamental remodeling processes of ECM as novel rapid response to high glucose treatment. Among others, Osteopontin (SPP1) as well as its interacting integrins were significantly downregulated and organotypic retinal explant culture confirmed the selective loss of SPP1 in RMG upon treatment. Since SPP1 in the retina has been described neuroprotective for photoreceptors and functions against experimentally induced cell swelling, it´s rapid loss under diabetic conditions may point to a direct involvement of RMG to the early neurodegenerative processes driving DR. Data are available via ProteomeXchange with identifier PXD015879.

1 **High glucose treatment promotes extracellular matrix**

2 **proteome remodeling in Müller glial cells**

4 Sandra Sagmeister[1,2], Juliane Merl-Pham[1], Agnese Petrera[1], Cornelia A Deeg[2*], Stefanie M

5 Hauck[1*]

7 [1] Research Unit Protein Science and Metabolomics and Proteomics Core Facility, Helmholtz

8 Center Munich, German Research Center for Environmental Health GmbH, Munich, Germany

9 [2] Chair of Physiology, Department of Veterinary Sciences, LMU Munich, Martinsried, Germany

11 Corresponding Author:

12 Stefanie M Hauck

13 Email address: hauck@helmholtz-muenchen.de

14 Cornelia A. Deeg

15 Email address: deeg@tiph.vetmed.uni-muenchen.de

Abstract

19 **Background.** The underlying pathomechanisms in diabetic retinopathy (DR) remain

20 incompletely understood. The aim of this study was to add to the current knowledge about the

21 particular role of retinal Müller glial cells (RMG) in the initial processes of DR.

22 **Methods.** Applying a quantitative proteomic workflow, we investigated changes of primary

23 porcine RMG under short term high glucose treatment as well as glycolysis inhibition treatment.

24 **Results.** We revealed significant changes in RMG proteome primarily in proteins building the

25 extracellular matrix (ECM) indicating fundamental remodeling processes of ECM as novel rapid

26 response to high glucose treatment. Among others, Osteopontin (SPP1) as well as its interacting

27 integrins were significantly downregulated and organotypic retinal explant culture confirmed the

28 selective loss of SPP1 in RMG upon treatment. Since SPP1 in the retina has been described

29 neuroprotective for photoreceptors and functions against experimentally induced cell swelling,

30 it´s rapid loss under diabetic conditions may point to a direct involvement of RMG to the early

31 neurodegenerative processes driving DR. Data are available via ProteomeXchange with

32 identifier PXD015879.

33

Introduction

35 The worldwide prevalence for diabetes in adults is increasing and is predicted to exceed ten

36 percent of world population by 2040 (Ogurtsova et al. 2017). Diabetic retinopathy (DR) is a

37 severe and frequent comorbidity of diabetes and a leading cause of vision loss (Ducos et al.

38 2020; Graue-Hernandez et al. 2020; Leasher et al. 2016). However, the underlying

39 pathomechanisms remain to be comprehensively elucidated (Mesquida et al. 2019). DR was long

40 proposed to be mainly a microvascular disease, but is today perceived rather as a

41 neurodegenerative disorder in its early stages (Kadlubowska et al. 2016). Neurodegeneration

42 occurs even before any vascular alterations can be detected and cannot be reversed

43 (Kadlubowska et al. 2016). Thus, there is an urgent need to learn about initial pathomechanisms

44 involved in the early neurodegenerative process. Retinal Müller glial cells (RMG) are a major

45 source for neuroprotective signals (Del Rio et al. 2011; Hauck et al. 2008; Hauck et al. 2014)

46 also in the diabetic mouse retina (Fu et al. 2015). Thus, the novel concept of modulating RMG to

47 improve or re-establish retinal function is gaining increasing attention. A detailed understanding

48 of RMG participation in the onset of neurodegeneration could guide novel therapeutic

49 intervention strategies and, in best case, help prevent neurodegeneration.

50 The retina is composed of a complex network of highly specialized cells (Mazade & Eggers

51 2020). RMG are the dominant macroglial cell type within the retina and retinal health depends

52 on their undisturbed functions (Bringmann et al. 2006). RMG seem to be fundamentally involved

53 in pathologic mechanism of DR (Coughlin et al. 2017). They mediate the local inflammatory

54 response, trigger pathological neovascularization and fibrosis, participate in damage of blood

55 retinal barrier and downregulate potassium channels vital to retinal fluid homeostasis and

56 synaptic function (Coughlin et al. 2017; Sorrentino et al. 2016; Subirada et al. 2018). However,

57 little is known about the exact mechanism in RMG and changes on protein level have not yet

58 been studied in DR (McDowell et al. 2018).

59 Due to the high anatomical and functional similarities of pig and human eyes, pig ocular tissue

60 has proven a promising model for translational research (Giese et al. 2020; Kleinwort et al. 2017;

61 Menduni et al. 2018; Renner et al. 2020). While other animal models fall short in mimicking the

62 clinical background of DR in man (Mi et al. 2014), the diabetic INS^{C94Y} transgenic pig is the first

63 model to represent a broad variety of the human retinal pathology (Kleinwort et al. 2017;

64 Weigand et al. 2020). We hence established a cell culture model for DR on isolated porcine

65 RMG by applying diabetic conditions *in vitro*. Hyperglycemia is considered as major trigger of

66 pathological events in DR (Mathebula 2018) and streptozotocin-induced diabetes is known to

67 increase retinal glucose levels in diabetic rats (Ola et al. 2006; Zhang et al. 2003). We therefore

68 applied short term high glucose treatment to simulate early hyperglycemic conditions in diabetes.

69 To meet another form of disturbed glucose metabolism, we also applied 2-deoxyglucose

70 treatment to simulate glycolysis inhibition (Valdes et al. 2016). There are indications that

71 decreased glycolysis or inactivity of glycolytic enzymes are another critical matter in the

72 development of DR in diabetic rats (Kanwar & Kowluru 2009; Ola et al. 2006; Thomas et al.

73 2019).

74 In this study, we explored proteomic changes of porcine RMG in a diabetic cell culture model

75 and contribute to understanding RMG mediated pathomechanisms in DR. Studying RMG

76 responses to short term high glucose and glycolysis inhibition treatment on protein level allowed

77 us to assess initial involvement of RMG in early stages of DR. The proteomic data was

78 confirmed by immunohistochemical staining on porcine retinal organotypic explant cultures.

79

80 Materials & Methods

81 **Preparation of primary RMG**

82 No experimental animals were used in this study, eyes from healthy adult pigs were received

83 fresh from a local abattoir. The eyes were removed from the animals within five minutes after

84 death and kept on ice in CO_2-independent medium (Thermo Fisher Scientific, Ulm, Germany)

85 until preparation started within one hour. Collection and use of porcine eyes from the abattoir

86 was approved for purposes of scientific research by the appropriate board of the veterinary

87 inspection office Munich, Germany (permit number: DE 09 162 0008-21). Eight neuroretinae

88 from eight animals were prepared and primary RMG were isolated as previously described

89 (Hauck, et al., 2003). Briefly, major blood vessels were removed, each retina was mechanically

90 cut and retinal pieces were washed twice in Ringer's solution (Millipore Sigma, Darmstadt,

91 Germany). Dissociation was obtained by treating each retina with 2.2 U of activated papain

92   (Worthington Biochemical, Troisdorf, Germany) for 12 minutes at 37°C. Papain enzyme activity

93   was stopped by the addition of DMEM Glutamax (Thermo Fisher Scientific) with 10% fetal calf

94   serum (Thermo Fisher Scientific). Then, 160 Kunitz-units of DNase (Millipore Sigma,

95   Darmstadt, Germany) was added and the tissue was further dissociated by gentle trituration using

96   a fire-polished Pasteur pipette. Dissociated cells were pooled, resuspended and plated in six well

97   format (cells from about two retinae per six well plate) in DMEM Glutamax containing 5.6 mM

98   glucose in addition of 10% fetal calf serum and 1% Penicillin-Streptomycin (Thermo Fisher

99   Scientific). After 24 hours at 37 °C in 5% CO_2, medium was exchanged and debris, nonattached

100 or loosely attached cells were removed by agitation (panning). Cells were cultivated for two

101 weeks without passaging and DMEM Glutamax culture medium was exchanged every 48 to 72

102 hours. Under these treatment conditions, porcine RMG cells are rapidly dominating the culture

103 and reach purity and 80% confluence after two weeks in culture (Hauck et al. 2003).

104 The time point after which confluence is reached strongly depends on the total number of seeded

105 cells. We spread the cells derived from two porcine eyes onto one 6well culture dish and

106 reproducibly reach 80% confluence after 14 days (100% confluence is never reached in these

107 cultures). We chose this time point for our studies because this was the earliest consistent time

108 point with reasonably high cell yields for proteomic workflows. However, growth of RMG *in*

109 *vitro* goes along with trans-differentiation during culturing concomitant with strong

110 downregulation of prototype RMG marker proteins, like glutaminsynthetase (GS) (Hauck et al.,

111 2003). The remaining expression of GS after only 7 days in culture (Hauck et al., 2003) is mainly

112 due to remaining resting cells which have not yet started growing (and simultaneously loosing

113 RMG markers). Since the mixture of non-growing and growing, yet de-differentiated cells is a

114 rather unstable experimental condition, we chose the time point 14 days, where the cells appear

115 homogeneously fibroblast-like, even though they have undergone trans-differentiation.

116 Cells were imaged by differential interference contrast on a Leica DMi8 microscope with the HC

117 PL Fluotar L 20x/0.40 DRY objective lens using a Leica DFC365FX-722433014 camera and

118 processed by the Leica Application Suite LASX (version 3.03, Leica, Wetzlar, Germany) (Fig1).

119 **Diabetic treatment of RMG**

120 Experiments were performed after 14 days in culture when cells reached a confluence of

121 approximately 80%. Diabetic treatment was performed for 72 hours, with replacement of the

122 respective culture medium every 24 hours. The cells under normoglycemic conditions (n=6

123 replicates, represented by different culture wells) were incubated at physiologic glucose level of

124 5.6 mM resembling the physiologic blood glucose level in human and porcine species (Renner,

125 et al., 2013). The cells under high glucose treatment conditions aiming to simulate

126 hyperglycemic conditions (n=6 replicates) were cultured with 35 mM glucose representing a

127 severe hyperglycemic state in diabetic patients (Yu et al. 2008; Zhu et al. 2015) by addition of

128 sterile filtered D-glucose (Millipore Sigma, Darmstadt, Germany). The cells under glycolysis

129 inhibition (n=6 replicates) were cultured under normoglycemic conditions with addition of 20

130 mM 2-deoxy-D-glucose (2-DG, Millipore Sigma, Darmstadt, Germany) during the last 24 of the

131 72 hours. 2-DG is a synthetic glucose analog that is assimilated and subsequently phosphorylated

132 by mammalian RMG *in vitro* (Poitry-Yamate & Tsacopoulos 1991; Toft-Kehler et al. 2017).

133 Uptake of 2-DG in mammalian (cancer) cells competes with glucose, as it is transferred by

134 glucose transporters (GLUTs) (Zhang et al. 2016). Phosphorylated 2-DG cannot be further

135 metabolized and accumulates leading to non-competitive inhibition of hexokinase, thus

136 disrupting glycolysis. In mouse retinae, a concentration of 1 mM 2-DG in the absence of glucose

137 is sufficient to almost completely disrupt energy production *ex vivo* within 45 minutes (Chertov

138 et al. 2011). In the presence of glucose, 2-DG was applied in a ratio of 1:1 competing glucose to

139 achieve glycolysis inhibition within 24 hours (Valdes et al. 2016). In this experiment we applied

140 an about 3.5 times excess of 2-DG compared to the glucose level to achieve glycolysis inhibition

141 (20 mM 2-DG and 5.6 mM glucose). Wells representing the different treatments were

142 randomized across three six well plates. Viability of cells at the end of the experiment was

143 examined under microscope and estimated over 80%.

144

145 **Sample preparation for mass spectrometry**

146 After treatment, cells were washed trice in ice cold phosphate buffered saline (PBS). Plates were

147 put on ice and 100 μl lysis buffer (PBS with 1% NP40, Roche Diagnostics, Mannheim,

148 Germany) was added per well. After two minutes of incubation, cells from each well were

149 scraped and collected separately. Lysis was performed by shear force and ultrasonication

150 followed by centrifugation for ten minutes at 10.000 rcf. Protein concentration was determined

151 by Bradford assay and equal total protein amounts (10 μg) per replicate were digested with a

152 modified FASP procedure (Grosche et al. 2016; Wisniewski et al. 2009). Briefly, protein lysates

153 were diluted with ammonium bicarbonate buffer (Millipore Sigma, Darmstadt, Germany) to a

154 final volume of 400 μl, followed by reduction using 1 μl of 1 M dithiothreitol (Millipore Sigma,

155 Darmstadt, Germany) for 30 min at 60 °C. After cooling down to room temperature, 8 M urea

156   buffer pH 8.5 (Millipore Sigma, Massachusetts, USA) was added to a final volume of 1 ml and

157   proteins were carbamidomethlylated with 10 µl of 300 mM iodoacetamide (Millipore Sigma,

158   Darmstadt, Germany) for 30 minutes at room temperature in the dark. Two µl of 1 M

159   dithiothreitol was added to quench unreacted iodoacetamide, and protein lysates passed 30 kDa

160   centrifugal filters, Vivacon 500 (Sartorius, Göttingen, Germany). After washing three times with

161   200 µl of urea buffer and three times with 100 µl of 50 mM ammonium bicarbonate buffer, the

162   proteins on the filters were subjected to a two hours digest at room temperature with 0.5 g of

163   Lysyl Endopeptidase (Wako, Osaka, Japan) followed by tryptic digest (1g of trypsin, Promega,

164   Madison, USA) over-night at 37 °C. Peptides were collected by centrifugation through the filter

165   and acidified with trifluoroacetic acid (Applied Biosystems, Foster City, USA) to a final pH 2.

166   **LC-MS/MS Analysis**

167   Approximately 0.5 µg of peptides per sample were measured in a randomized fashion on a Q-

168   Exactive HF mass spectrometer online coupled to an Ultimate 3000 nano-RSLC (Thermo Fisher

169   Scientific, Ulm, Germany) in data-independent acquisition (DIA) mode as previously described

170   (Lepper et al. 2018; Mattugini et al. 2018). Briefly, peptides were loaded automatically on a trap

171   column (300 µm inner diameter × 5 mm, Acclaim PepMap100 C18, 5 µm, 100 Å; LC Packings,

172   Sunnyvale, USA) prior to C18 reversed phase chromatography on the analytical column

173   (nanoEase MZ HSS T3 Column, 100Å, 1.8 µm, 75 µm x 250 mm; Waters, Milford, USA) at 250

174   nl/min flow rate in a 105 minute non-linear acetonitrile gradient from 3 to 40% in 0.1% formic

175   acid. Profile precursor spectra from 300 to 1650 m/z were recorded at 120,000 resolution and a

176   maximum injection time of 120 ms for achieving an automatic gain control (AGC) value of 3e6.

177   Subsequently fragment spectra were recorded in 37 overlapping DIA isolation windows (1 Da

178   overlap on each side) of variable size covering in total 300 to 1650 m/z, each at 30,000

179   resolution with an AGC target of 3e6 and a normalized collision energy of 27.

180   **Quantitative Analysis**

181   The recorded raw files were analyzed using the Spectronaut software (version 12, Biognosys,

182   Schlieren, Switzerland (Bruderer, et al., 2015, Bruderer, et al., 2016) with a peptide identification

183   false discovery rate setting of < 1%, using an in-house pig spectral library which was generated

184   using Biognosys Spectronaut 12 and the Ensembl Pig database (release 75, Sscrofa10.2).

185   Quantification was based on MS2 area levels of all unique proteotypic peptides per protein

186   fulfilling the percentile 0.2 setting. Normalized protein quantifications were exported and used

187 for calculations of fold-changes and significance values. Each group originally included six

188 replicates; in the normoglycemic control group two replicates were excluded due to a deviating

189 abundance response that could not be solved by normalization.

190 **Statistics, Graphics, Principal component analysis, Pathway enrichment analysis, Volcano**

191 **plots, Venn diagram and Network generation**

192 To analyze the differential protein abundance between the diabetic treatment groups and the

193 control group, a two-tailed, unpaired student`s t-test was performed on log2 transformed

194 normalized abundances. Proteins were considered significantly changed upon the following

195 criteria: (a) quantified with ≥ 2 unique peptides and (b) t-test p-value < 0.05. Additionally, a fold

196 change cut-off of ≥ 1.33-fold or ≤ 0.75-fold was applied. To justify the chosen fold change cut-

197 off, we calculated the average variation coefficient CV of the individual groups (resulting in

198 average CVs of 13.2% in the normoglycemic, 12.0% in the high glucose and 14.1% in the

199 glycolysis inhibition group) and chose the fold change cut-off to exceed twice the maximal group

200 CV.

201 The workflow (Fig1) was designed using the medical image bank Servier Medical Art, which is

202 available under the Creative Commonslicense CC-BY (https://smart.servier.com/).

203 Pathway enrichment analysis (Fig2) was performed separately for the hyperglycemic and the

204 glycolysis inhibition treatment group with Genomatix Generanker (Genomatix Software GmbH,

205 Munich, Germany, http://www.genomatix.de) using EIDorado (version 04-2019) and Literature

206 Mining Database (version 02-2019). Inclusion criteria for proteins were (a) p-value < 0.05, (b)

207 quantification with ≥ 2 unique peptides and (c) a ≥ 1.33 fold or ≤ 0.75-fold differential

208 abundance level. Gene names of input proteins were uploaded using H. sapiens as the organism

209 for background list.

210 To illustrate overlap of proteins from the high glucose and the glycolysis inhibition treatment

211 groups (Fig3a) that fulfil criteria (a) p-value < 0.05 and (b) quantification with ≥ 2 unique

212 peptides from high glucose and glycolysis inhibition group and (c) a ≥ 1.33-fold or ≤ 0.75-fold

213 differential abundance level in these both groups in comparison to the normoglycemic group, we

214 employed BioVenn (Tim Hulsen, http://www.biovenn.nl) (Hulsen, et al., 2008).

215 For generation of the network of proteins (Fig3b), we used STRING (Search Tool for the

216 Retrieval of Interacting Genes/ Proteins, version 11.0, STRING consortium 2017, https://string-

217 db.org) which belongs to the ELIXIR's Core Data Resources (Szklarczyk et al. 2019). STRING

218 was employed using "highest confidence" regarding the interaction score, with a score limit of

219 0.9 describing the approximate probability that a predicted link exists between two proteins in

220 the same metabolic map in the KEGG database (release 90.1). Additionally, disconnected nodes

221 were hidden while the thickness of the connection lines indicates the strength of the data support.

222 All of the presented connection lines reaching the maximum thickness indicated the maximal

223 strength of the data support. As input format we chose gene names and H. sapiens as organism.

224 **Porcine neuroretinal organotypic explant cultures**

225 Healthy adult porcine eyes were provided by a local abattoir, removed from the animals within

226 five minutes after death and kept on ice in CO_2-independent medium until preparation was

227 completed within three hours. One explant was dissected per eye, and all of the eyes were

228 obtained from different animals. Neuroretinal explants were dissected as described (Taylor et al.

229 2014) with some modifications. The opened eyecup was filled with prewarmed CO_2-independent

230 medium and the neuroretina was carefully removed from retinal pigment epithelium by very

231 softly flushing medium between the two structures. To ensure correct orientation concerning

232 retinal topography, neuroretina was properly teased back into the original position with a

233 forceps. We carefully excised circular tissue pieces of 6 mm diameter with a biopsy punch (PFM

234 Medical, Köln, Germany) from the dorso-nasal position of the optic disc (Fig4).

235 Free floating neuroretinal pieces were carefully collected with the upper (large) end of a pasteur

236 pipette connected to a pasteur pipette bulb at the broken lower end and positioned onto 0.4 μm

237 culture plate inserts (Thermo Fisher Scientific, Roskilde, Denmark) with the inner limiting

238 membrane side facing the insert membrane and thus providing inner retinal support (Taylor et al.

239 2014). Inserts were placed in six well plates filled with1.5ml RPMI 1640 medium (Thermo

240 Fisher Scientific, Ulm, Germany) containing 11 mM glucose and supplemented with 10% fetal

241 calf serum and 0.2% Penicillin-Streptomycin and respective treatment additives. A drop of

242 medium was placed at the air interface on top of each explant and explants were incubated at 37

243 °C in 5% CO_2.

244 **Treatment of explants**

245 Treatment started immediately after dissection. During the 72 hours of treatment, culture

246 medium in the chamber below the explant as well as the drop placed on top of the explant was

247 replaced every 24 hours. The normoglycemic group (n=4 biological replicates, represented by

248 explants from different eyes and animals) was maintained with a glucose level of 11 mM as

249   included in RPMI 1640 medium. The hyperglycemic group (n=4 biological replicates) was

250   cultured under high glucose conditions containing 70 mM glucose due to addition of sterile

251   filtered D-glucose. This concentration was defined in consideration of the factor of 6.25 between

252   normoglycemic and high glucose group that was employed in the isolated RMG cell experiment

253   before (5.6 mM normoglycemic, 35 mM high glucose, 6.25 fold increase). To investigate an

254   osmotic effect independent of the metabolic effects of glucose (Yu et al. 2017), we included an

255   osmotic control group (n=4 biological replicates) containing 11 mM of glucose and 59 mM D-

256   mannose (Millipore Sigma, Darmstadt, Germany) to achieve the same osmolarity like in the high

257   glucose group. Explants representing the glycolysis inhibition group (n=4 biological replicates)

258   were cultured with levels of 11 mM glucose with addition of 40 mM 2-DG within the last 24 of

259   the 72 hours. This concentration was determined to achieve an about 3.5-fold overdose of 2-DG

260   compared to glucose similar to the RMG experiment (which was 20 mM 2-DG with 5.6 mM

261   glucose).

262   **Immunohistochemistry of explants**

263   After 72 hours of treatment, explants were fixated, dehydrated and embedded for cryo sectioning

264   adapted from a protocol provided by Linnea Taylor, Ophthalmology Department, Medical

265   Faculty, Lund University (Taylor et al. 2014). Briefly, prechilled (4 °C) paraformaldehyde (PFA)

266   4% (BosterBio, Pleasanton, USA) was drop-wise added to explants still adherent to the insert

267   membrane over a time period of minimal five minutes until they were completely covered with

268   PFA and fixation continued for three hours at 4 °C. PFA was removed and explants were washed

269   three times with prechilled phosphate buffer (PB; 0.1 M, pH 7.4). Then each explant was excised

270   with 8 mm biopsy punch (PFM Medical, Köln, Germany) and transferred with the membrane to

271   a flat biopsy capsules (Cell Path, Newton, UK). Cryopreservation was performed by incubating

272   in PB-containing 15% sucrose (Millipore Sigma, Darmstadt, Germany) for four hours followed

273   by incubation in PB-containing 30% sucrose overnight at ambient temperature. Explants were

274   taken from the capsule, moved to 12 mm x 8 mm embedding molds (Polyscienes, Niles, USA),

275   cryo-embedded together with the membrane in OCT medium (Thermo Fisher Scientific, Ulm,

276   Germany) and stored at -80°C. Cryo-sections were collected from the center parts of each

277   explant at 18μm thickness, mounted on coated slides (Superfrost Plus, Thermo Scientific, Ulm,

278   Germany) and stored at -20°C.

279 Slides were defrosted at room temperature for 20 minutes and washed with PB trice for ten

280 minutes each. To avoid unspecific antibody binding, sections were blocked in Tris-buffered

281 saline containing 0.1% Tween 20 (Serva, Heidelberg, Germany, TBS-T), 1% bovine serum

282 albumin (Biomol, Hamburg, Germany) and 5% goat serum (Abcam, Berlin, Germany) for one

283 hour at ambient temperature. Sections were then co-incubated overnight at 4 °C with rabbit anti-

284 SPP1 (1:250, OriGene, Herford, Germany) and mouse anti-vimentin (1:50, Millipore Sigma,

285 Darmstadt, Germany) diluted in TBS-T with 1% bovine serum albumin and 5% goat serum,

286 followed by co-incubation with goat anti-rabbit IgG AlexaFluor 488 and goat anti-mouse IgG

287 AlexaFluor 568 (each 1:500, Thermo Fisher Scientific, Ulm, Germany) for 90 minutes at

288 ambient temperature. Between primary and secondary resp. after secondary antibody incubations

289 sections were washed three times each with PB for 10 minutes. After counterstaining with

290 Hoechst (1:10,000, Thermo Fisher Scientific, Ulm, Germany) for 10 minutes at ambient

291 temperature, coverslips were mounted in aqueous FluorSave cover medium (Thermo Fisher

292 Scientific, Ulm, Germany) and photographed on a Leica DMi8 microscope with the HC PL APO

293 40x/0.95 DRY objective lens. Filter cubes for GFP, Texas Red and DAPI detections were used

294 (JH Technologies). All images were captured using a Leica DFC365 FX camera, and constant

295 settings for gain and exposure time were maintained for all sections within an experimental

296 setup. Images were processed by the Leica Application Suite LASX (version 3.03, Leica). As

297 control, three sections per group from different explants were stained under equal conditions

298 with anti-rabbit-IgG (1:1,000, Abcam, Berlin, Germany) instead of anti-SPP1; no unspecific

299 labeling was observed.

300

301 **Results**

302 **Overrepresentation of ECM-associated biological processes in RMG under diabetic culture**

303 **conditions**

304 We isolated primary porcine RMG from pig eyes, applied the diabetes short term treatment and

305 investigated proteome-wide changes applying a mass spectrometric work flow (Fig. 1). A total of

306 2744 proteins quantified with ≥ 2 unique peptides were detected across in all treatment groups

307 and replicates (Supplemental table 1).

308 In the high glucose treatment group, a total of 464 proteins were significantly differently

309 abundant compared to the normoglycemic control group (Fig. 2a, protein-dots above the

310   reference line for p-value cut-off, supplemental table 2), thereof 103 proteins met the additional

311   criterion of fold change cut-off (Fig. 2a, colored protein-dots beyond both reference lines for fold

312   change cut-off). Pathway enrichment analysis of these 103 proteins revealed the top ten

313   biological processes that were significantly enriched with a functional relationship to the input

314   proteins (Fig. 2b). The three highest ranking pathways are strongly associated with extracellular

315   matrix function, namely "collagen fibril organization", "extracellular matrix organization" and

316   "extracellular structure organization" (Fig. 2b, supplemental table 3). Accordingly, among the

317   changed proteins were 19 members of the ECM (supplemental table 2, according to the human

318   matrisome database, http://matrisomeproject.mit.edu (Naba, et al., 2016); Fig2a, labeled with

319   gene symbols) of which the majority (16) showed lower abundance levels in the high glucose

320   treatment group compared to the normoglycemic control group.

321   In the glycolysis inhibition treatment group, altogether 800 proteins exhibited significant changes

322   in abundance levels compared to the normoglycemic control group (Fig. 2c, protein-dots above

323   the reference line for p-value cut-off, supplemental table 4;), of which 240 proteins additionally

324   met the fold change cut-off (Fig. 2c, colored protein-dots beyond both reference lines for fold

325   change cut-off). Again, pathway enrichment analysis of these 240 proteins pointed to an

326   overrepresentation of proteins belonging to the context of extracellular matrix, which was

327   demonstrated by the three most significantly overrepresented biological processes (Fig. 2d,

328   namely "extracellular structure organization", "collagen fibril organization" and "extracellular

329   matrix organization"; supplemental table 5). Correspondingly, there were 34 ECM members

330   among the input proteins (supplemental table 4, according to the human matrisome database;

331   Fig. 2c labeled with gene symbols), with the majority (28) once again showing lower abundance

332   levels in the glycolysis inhibition treatment group compared to the normoglycemic control

333   group. Interestingly, secreted phosphoprotein 1 (SPP1) appeared in both diabetes-like conditions

334   as one of the top changed candidates.

335   **Downregulation of ECM organization and cell adhesion processes under diabetic culture**

336   **conditions**

337   Both diabetic treatments caused a similar pattern of highly overrepresented processes when

338   compared to the normoglycemic control. Hence, we aimed to clarify if this could be linked to a

339   similar alteration in abundance level of particular proteins or groups of proteins. There were

340   differences in the proteins with changed abundance between diabetic conditions, but 65 of all

341 differently abundant proteins overlapped (Fig. 3a). We concluded that these 65 proteins have

342 fundamental roles in RMG metabolism, since they reacted consistently to different changes

343 applied to glucose metabolism by our experimental treatments. We next performed a protein

344 enrichment analyses with STRING, applying strict evaluation criteria to investigate the major

345 functions of these 65 proteins. These analyses confirmed enriched interactions of proteins of the

346 biological process "ECM organization" and additionally defined the biological process "cell

347 adhesion" (Fig. 3b, according to the Gene Ontology term of biological processes). Sixty-two of

348 65 proteins changed their abundance in the same way, so either decreasing (39 proteins) or

349 increasing (23 proteins) their abundance levels in both treatment groups compared to the control

350 group. All of the proteins belonging to the "ECM organization" and "cell adhesion" biological

351 process in the STRING network are proteins with decreased abundance in both treatment groups

352 compared to the normoglycemic control group. That points to a downregulation of both

353 processes in high glucose and glycolysis inhibition treatment.

354 Some of the candidates have functions in ECM organization as well as in cell adhesion. Among

355 them is SPP1 (Fig. 3b), that interacts in both pathways with collagen-α-chains, fibronectin and

356 the alpha integrins ITGA5, ITGA8, ITGAL (Fig. 3b, supplemental tables 2 and 4). We therefore

357 decided to further investigate SPP1 in our hyperglycemia model.

358 **RMG-associated SPP1 expression pattern selectively diminished in retinal explants under**

359 **diabetic culture conditions**

360 SPP1 was consistently decreased in both diabetic conditions and belongs to several

361 overrepresented biological processes in the dataset. Earlier, SPP1 was shown to play a key role

362 in RMG mediated pathogenesis in an inflammatory eye disease (Deeg, et al., 2011). Further,

363 SPP1 was recently found to be secreted by porcine RMG *in vitro*, exhibiting a survival-

364 promoting effect on porcine retinal ganglion cells *in vitro* (Ruzafa et al. 2018b).

365 To analyze SPP1 in the context of the retinal network of RMG cells, we next used porcine retinal

366 explants as a model. We took pieces from the visual streak (Fig. 4a), a region of the porcine

367 retina which is characterized by very high densities of cones and ganglion cells, in a ratio that is

368 also found in humans (Garca, et al., 2005, Hendrickson and Hicks, 2002). Explants were cultured

369 on the fluid/air interface on a polycarbonate membrane (Fig. 4b). In reference to the isolated

370 porcine RMG, short term diabetic treatment was applied. An osmotic control group was included

371   to determine the osmotic effect independently of the effect of high glucose or glycolysis

372   inhibition to the explants (Fig. 4b).

373   Since SPP1 expression patterns in porcine retina were not reported so far to our knowledge, we

374   initially examined it`s distribution by immunohistochemical fluorescence staining of porcine

375   retinal organotypic explant cultures after three days *in vitro* under normoglycemic conditions

376   (Fig. 5).

377   SPP1 was detected at the level of photoreceptor outer segments (POS) and in the inner

378   neuroretina in the area of the ganglion cell layer (GCL) and nerve fiber layer (NFL) (Fig. 5, top,

379   left panel). Vimentin was used as marker for RMG and its characteristic RMG morphology (Fig.

380   5, top, mid panel). Double labeling of SPP1 with vimentin revealed co-localization along RMG

381   processes and endfeet in the inner neuroretina (Fig. 5, top, right panel). This co-localization in

382   the area of the GCL and NFL suggests RMG-associated SPP1 expression also in the *ex vivo*

383   retinal system.

384   We then aimed to investigate if SPP1 expression in the *ex vivo* retinal system is downregulated in

385   response to diabetic culture conditions. In all four conditions, vimentin was characteristically

386   expressed in RMG processes throughout the inner retina from the endfeet that build the inner

387   limiting membrane to the outer plexiform layer (Fig. 5, mid panels, vimentin red). In osmotic

388   control and in both diabetic conditions (high glucose and glycolysis inhibitions), the RMG-

389   associated SPP1 diminished in comparison to the normoglycemic cultured explants (Fig. 5, left

390   panels, SPP1 green; overlay with vimentin staining: right panels). Interestingly, SPP1 staining at

391   the level of photoreceptor outer segments remained unaltered in all conditions, indicating a

392   specific RMG response.

393

Discussion

395   Diabetes mellitus is currently one of the major health concerns with nearly half a billion people

396   affected worldwide and a permanently increasing prevalence (Saeedi et al. 2019). Chronic

397   hyperglycemia and its consequences are the main issues of diabetes mellitus (Renner et al. 2013).

398   Diabetic retinopathy as a microvascular complication is also one of the fastest growing diseases

399   worldwide, leading to blindness and greatly impairs quality of life in affected patients (Harding

400   et al. 2019). To date, the mechanisms leading to retinal damage are not well understood.

401 Appropriate animal models to address the pathogenesis of diabetic retinopathy are scarce to date,

402 because traditional animal models in rodents lack translational value because of significant

403 differences in physiological, anatomical and immunological aspects. The pig recently evolved as

404 a favorable model for diabetes given the marked similarity with the humans with respect to the

405 developed pathophysiological features (Cole & Florez 2020; Kleinwort et al. 2017; Renner et al.

406 2020; Renner et al. 2013). RMG is the most important glial cell in the retina where it plays a

407 central role (Bringmann et al. 2006; Bringmann & Wiedemann 2012) in the pathology of DR,

408 RMG seem to be fundamentally involved. However, the molecular mechanisms of pathological

409 changes to and initiated by this specific cell type are not well understood (McDowell et al. 2018).

410 Recently, a proteomic study in diabetic patients demonstrated retinol binding protein-3 to control

411 glucose transport in RMG and thus development of DR (Yokomizo et al. 2019). This study

412 highlights not only the successful application of proteomic techniques to elucidate molecular

413 pathomechanisms in DR, but also the important role of RMG in pathologic processes of diabetic

414 retina. To the best of our knowledge proteome-wide responses of RMG to diabetes-like

415 metabolic situations have not been studied before and by using a comprehensive, differential

416 proteomic analysis in our primary RMG cell culture model (Hauck et al. 2003), we were able to

417 investigate specific mechanisms attributed to this particular cell type. Short term treatment in cell

418 culture allowed to shed light on the mechanisms underlying the initial phases of disturbed

419 glucose metabolism. Applying a differential proteome analysis approach, we observed highly

420 significant proteome changes in cells cultured under two different treatment regimens designed

421 to mimic fluctuating glucose levels naturally occurring in diabetes. A total of 65 proteins showed

422 a significant differential expression upon both diabetes-like conditions. A pathway enrichment

423 analysis of the proteins with altered abundance revealed an enrichment of ECM associated

424 pathways, with a hinted downregulation of ECM organization and cell adhesion. Decreased

425 production of ECM proteins under diabetic conditions could explain our previous finding of the

426 disruption of the inner limiting membrane (ILM) in a diabetic pig model resulting in

427 accumulation of hard exudates and cotton-wool spots, which are common features of

428 proliferative neovascularization (Kleinwort et al. 2017).

429 The ILM is a thin sheet composed of ECM proteins at the inner surface of the retina closely

430 connected to RMG endfeet (Syrbe et al. 2018). There is evidence that human RMG produce

431 ECM proteins suggesting their role in the ILM assembly (Ponsioen et al. 2008). The present data

432   point toward a remodeling of ECM proteins which potentially destabilizes the ILM thereby

433   impairing its integrity in DR. Further support to our hypothesis on RMG involvement in de-

434   stabilizing ILM is provided by the observed downregulation of integrins, which are key factors

435   for the correct assembly and function of ILM (Halfter et al. 2008).

436   Since the retina comprises a highly sophisticated neuronal network of many specialized cells in

437   close interaction, we aimed to confirm our findings in a model which closely resembles in vivo

438   conditions. Hence we established porcine organotypic retinal explants cultures which preserve

439   the cellular architecture and functional interactions physiologically present in the tissue hence

440   providing an adequate and comprehensive model of the retina (Schnichels et al. 2019).

441   In this study, porcine retinal explants were excised from the visual streak, a region of the porcine

442   retina which is characterized by high densities of cones and ganglion cells (Garca et al. 2005;

443   Hendrickson & Hicks 2002). The region dorso-nasal the optic disc within the visual streak

444   contains the highest cone numbers and thus resembles the human macula (Hendrickson & Hicks

445   2002; Kleinwort et al. 2017). We therefore examined a retinal region with a similar cellular

446   distribution like the human macula to use the advantage of the porcine model to learn about

447   human macula diseases.

448   We identified SPP1 (synonym osteopontin) as a major changed candidate in our study. SPP1 is

449   an interesting molecule with pleiotropic functions (Ruzafa et al. 2018a). The function in the

450   retina is not entirely clear to date (Ruzafa et al. 2018a). SPP1 influences cell survival and

451   attachment, cell migration, inflammation, migration and homeostasis after injury (Ruzafa et al.

452   2018a). In this study, SPP1 disappeared significantly and rapidly in short term hyperglycemic

453   conditions in cell culture models and likewise in organotypic cultures. Although the exact

454   implications for diabetic retinopathy remain open at this point, the loss of a SPP1, which has

455   been described to rescue photoreceptors and to be induced by neuroprotective factor GDNF (Del

456   Rio et al. 2011), is an important finding of our study and deserves further investigation in our

457   opinion. Interestingly, the loss of protein abundance was not limited to SPP1, but was also

458   observed for its known interactors, the integrins (Yang et al. 2019).

459   Here, among other integrins, ITGB1 was downregulated under simulated diabetic conditions.

460   Conditional deletion of ITBG1 in mouse brain leads to partial gliosis of astrocytes (Robel et al.

461   2009). Gliosis is generally considered as a protective response of glial cells to harmful insults

462   (Bringmann et al. 2006; Burda & Sofroniew 2014) and occurs in RMG probably in an early stage

463   of DR (Vujosevic et al. 2015). However, in contrast to the observed downregulation of ITGB1,

464   GFAP and vimentin, two prototype markers of gliosis, were not changed by modifying glucose

465   levels in RMG (see supplemental table 1). Therefore, we speculate that changes in ECM proteins

466   related to gliosis could be triggered by high glucose treatment even before upregulation of

467   intermediate filament proteins (Liu et al. 2016), as well established marker for reactive RMG

468   gliosis (Subirada et al., 2018).

469   Our results may indicate an involvement of RMG in the neurodegenerative processes in early

470   DR, because SPP1 protein was consistently found less abundant in cultured RMG under diabetic

471   treatment conditions. To date, we do not know the molecular mechanism leading to decrease in

472   SPP1 in these conditions. Potential effects of hyperglycemia in diabetes range from specific

473   metabolic effects, through non-enzymatic glycation, glycoxidation, lipoxidation and osmotic

474   stress (Yu et al. 2007). In our cell culture environment, mannose was applied to specifically

475   induce osmotic effects in the explants and to distinguish them from the other hyperglycemia-

476   induced mechanisms (Yu et al. 2007). Since the observed effects on the abundance of SPP1 also

477   occurred in the osmose control group, we speculate that alterations in the SPP1 protein levels

478   might result from a multi-causative osmotic stress. This report is the first to describe a RMG

479   specific SPP1 regulation in a high glucose and hyperosmolar state. Since the hyperglycemic

480   hyperosmolar state is a serious acute metabolic complication of diabetes mellitus (Umpierrez &

481   Korytkowski 2016), further experiments should unravel potential relations of hyperglycemic and

482   osmotic conditions that induce decrease in SPP1 levels.

483   Interestingly, it has been shown that supplemented SPP1 inhibits experimentally induced osmotic

484   swelling in *ex vivo* rat RMG (Wahl et al. 2013). Glial swelling is involved in pathology of

485   diabetic macula edema, a severe complication of DR (Coughlin et al. 2017; Daruich et al. 2018;

486   Graue-Hernandez et al. 2020; Wahl et al. 2013). We speculate that a decrease in SPP1 expression

487   level might contribute to RMG swelling in diabetic macular edema. In the retina of diabetic pigs

488   we observed a central swelling of the NFL (Kleinwort et al. 2017). It is reasonable to believe that

489   decreased expression of SPP1 could account for the swelling of glial cells as well as the

490   surrounding structures.

491   Noteworthy is the neuroprotective function of SPP1 in retina. In the porcine model, a pro-

492   survival effect of SPP1 on *in vitro* retinal ganglion cells (Ruzafa et al. 2018b) and on

493   photoreceptors (Del Rio et al. 2011) has been described. We believe that under diabetic

494   conditions, reduced expression of RMG-associated SPP1 might contribute to severe neuronal

495   damage in DR *in vivo*. Investigating whether neuronal survival in porcine retinal explants is

496   affected by RMG-associated SPP1 expression will be the focus of our future studies.

497   Interestingly, we have also previously found a significant downregulation of RMG-associated

498   SPP1 expression in retinas of horses with uveitis (Deeg et al. 2011). Collectively, these data

499   point to SPP1 being generally involved in retinal pathology.

500

501   **Conclusions**

502   Our findings suggest an initial involvement of RMG in DR. Perturbation with glucose levels

503   significantly alters many ECM proteins in RMG suggesting profound ECM remodeling; secreted

504   phosphoprotein 1 (SPP1) being one of these. Given the previously described neuroprotective role

505   of SPP1 and its inhibitory role on RMG cell swelling, SPP1 could hold potential as candidate

506   molecule for developing treatment strategies. Modulating SPP1 levels, as well as other

507   components of the ECM could help to prevent neurodegeneration in DR and RMG might

508   represent promising targets in such circumstances.

509

510   **Acknowledgements**

511   We would like to thank Linnea Taylor from the Ophthalmology Department, Medical Faculty,

512   Lund University for her help in establishing the porcine retinal explants in our lab and critical

513   discussions.

514

515   **Funding Information**

516   This work was funded by grants from the Deutsche Forschungsgemeinschaft: HAU 6014/5-1 (to

517   Stefanie M Hauck) und DE 719/7-1 (to Cornelia A Deeg) in the priority program SPP 2127.

518

References

521

Bringmann A, Pannicke T, Grosche J, Francke M, Wiedemann P, Skatchkov SN, Osborne NN, and Reichenbach A. 2006. Muller cells in the healthy and diseased retina. *Progress in Retinal and Eye Research* 25:397-424. 10.1016/j.preteyeres.2006.05.003

Bringmann A, and Wiedemann P. 2012. Müller Glial Cells in Retinal Disease. *Ophthalmologica* 227:1-19. 10.1159/000328979

Burda JE, and Sofroniew MV. 2014. Reactive gliosis and the multicellular response to CNS damage and disease. *Neuron* 81:229-248. 10.1016/j.neuron.2013.12.034

Chertov AO, Holzhausen L, Kuok IT, Couron D, Parker E, Linton JD, Sadilek M, Sweet IR, and Hurley JB. 2011. Roles of glucose in photoreceptor survival. *J Biol Chem* 286:34700-34711. 10.1074/jbc.M111.279752

Cole JB, and Florez JC. 2020. Genetics of diabetes mellitus and diabetes complications. *Nature Reviews Nephrology*. 10.1038/s41581-020-0278-5

Coughlin BA, Feenstra DJ, and Mohr S. 2017. Muller cells and diabetic retinopathy. *Vision Res* 139:93-100. 10.1016/j.visres.2017.03.013

Daruich A, Matet A, Moulin A, Kowalczuk L, Nicolas M, Sellam A, Rothschild P-R, Omri S, Gélizé E, Jonet L, Delaunay K, De Kozak Y, Berdugo M, Zhao M, Crisanti P, and Behar-Cohen F. 2018. Mechanisms of macular edema: Beyond the surface. *Progress in Retinal and Eye Research* 63:20-68. https://doi.org/10.1016/j.preteyeres.2017.10.006

Deeg CA, Eberhardt C, Hofmaier F, Amann B, and Hauck SM. 2011. Osteopontin and fibronectin levels are decreased in vitreous of autoimmune uveitis and retinal expression of both proteins indicates ECM re-modeling. *PLoS One* 6:e27674. 10.1371/journal.pone.0027674

Del Rio P, Irmler M, Arango-Gonzalez B, Favor J, Bobe C, Bartsch U, Vecino E, Beckers J, Hauck SM, and Ueffing M. 2011. GDNF-induced osteopontin from Muller glial cells promotes photoreceptor survival in the Pde6brd1 mouse model of retinal degeneration. *Glia* 59:821-832. 10.1002/glia.21155

Ducos C, Rigo M, Larroumet A, Delyfer M-N, Korobelnik J-F, Monlun M, Foussard N, Poupon P, Haissaguerre M, Blanco L, Mohammedi K, and Rigalleau V. 2020. Diabetic retinopathy in well-controlled type 2 diabetes: role of glycaemic memory. *Diabetes & Metabolism*. https://doi.org/10.1016/j.diabet.2020.03.005

Fu S, Dong S, Zhu M, Sherry DM, Wang C, You Z, Haigh JJ, and Le YZ. 2015. Muller Glia Are a Major Cellular Source of Survival Signals for Retinal Neurons in Diabetes. *Diabetes* 64:3554-3563. 10.2337/db15-0180

Garca M, Ruiz-Ederra J, Hernandez-Barbachano H, and Vecino E. 2005. Topography of pig retinal ganglion cells. *J Comp Neurol* 486:361-372. 10.1002/cne.20516

Giese IM, Schilloks MC, Degroote RL, Weigand M, Renner S, Wolf E, Hauck SM, and Deeg CA. 2020. Chronic Hyperglycemia Drives Functional Impairment of Lymphocytes in Diabetic INS (C94Y) Transgenic Pigs. *Front Immunol* 11:607473. 10.3389/fimmu.2020.607473

Graue-Hernandez EO, Rivera-De-La-Parra D, Hernandez-Jimenez S, Aguilar-Salinas CA, Kershenobich-Stalnikowitz D, and Jimenez-Corona A. 2020. Prevalence and associated risk factors of diabetic retinopathy and macular oedema in patients recently diagnosed with type 2 diabetes. *BMJ open ophthalmology* 5:e000304-e000304. 10.1136/bmjophth-2019-000304

Grosche A, Hauser A, Lepper MF, Mayo R, von Toerne C, Merl-Pham J, and Hauck SM. 2016. The Proteome of Native Adult Muller Glial Cells From Murine Retina. *Mol Cell Proteomics* 15:462-480. 10.1074/mcp.M115.052183

568   Halfter W, Dong S, Dong A, Eller AW, and Nischt R. 2008. Origin and turnover of ECM proteins
569   from the inner limiting membrane and vitreous body. *Eye (Lond)* 22:1207-1213.
570   10.1038/eye.2008.19
571   Harding JL, Pavkov ME, Magliano DJ, Shaw JE, and Gregg EW. 2019. Global trends in
572   diabetes complications: a review of current evidence. *Diabetologia* 62:3-16.
573   10.1007/s00125-018-4711-2
574   Hauck SM, Gloeckner CJ, Harley ME, Schoeffmann S, Boldt K, Ekstrom PA, and Ueffing M.
575   2008. Identification of paracrine neuroprotective candidate proteins by a functional
576   assay-driven proteomics approach. *Molecular & Cellular Proteomics : MCP* 7:1349-
577   1361. 10.1074/mcp.M700456-MCP200
578   Hauck SM, Suppmann S, and Ueffing M. 2003. Proteomic profiling of primary retinal Muller glia
579   cells reveals a shift in expression patterns upon adaptation to in vitro conditions. *Glia*
580   44:251-263.
581   Hauck SM, von Toerne C, and Ueffing M. 2014. The neuroprotective potential of retinal Muller
582   glial cells. *Lacrimal Gland, Tear Film, and Dry Eye Syndromes 3: Basic Science and*
583   *Clinical Relevance, Pts a & B* 801:381-387. 10.1007/978-1-4614-3209-8_48
584   Hendrickson A, and Hicks D. 2002. Distribution and density of medium- and short-wavelength
585   selective cones in the domestic pig retina. *Experimental eye research* 74:435-444.
586   10.1006/exer.2002.1181
587   Kadlubowska J, Malaguarnera L, Waz P, and Zorena K. 2016. Neurodegeneration and
588   Neuroinflammation in Diabetic Retinopathy: Potential Approaches to Delay Neuronal
589   Loss. *Current Neuropharmacology* 14:831-839. 10.2174/1570159x14666160614095559
590   Kanwar M, and Kowluru RA. 2009. Role of glyceraldehyde 3-phosphate dehydrogenase in the
591   development and progression of diabetic retinopathy. *Diabetes* 58:227-234.
592   10.2337/db08-1025
593   Kleinwort KJH, Amann B, Hauck SM, Hirmer S, Blutke A, Renner S, Uhl PB, Lutterberg K,
594   Sekundo W, Wolf E, and Deeg CA. 2017. Retinopathy with central oedema in an INS
595   (C94Y) transgenic pig model of long-term diabetes. *Diabetologia* 60:1541-1549.
596   10.1007/s00125-017-4290-7
597   Leasher JL, Bourne RR, Flaxman SR, Jonas JB, Keeffe J, Naidoo K, Pesudovs K, Price H,
598   White RA, Wong TY, Resnikoff S, Taylor HR, and Vision Loss Expert Group of the
599   Global Burden of Disease S. 2016. Global Estimates on the Number of People Blind or
600   Visually Impaired by Diabetic Retinopathy: A Meta-analysis From 1990 to 2010.
601   *Diabetes Care* 39:1643-1649. 10.2337/dc15-2171
602   Lepper MF, Ohmayer U, von Toerne C, Maison N, Ziegler AG, and Hauck SM. 2018. Proteomic
603   Landscape of Patient-Derived CD4+ T Cells in Recent-Onset Type 1 Diabetes. *Journal*
604   *of Proteome Research* 17:618-634. 10.1021/acs.jproteome.7b00712
605   Mathebula SD. 2018. Biochemical changes in diabetic retinopathy triggered by hyperglycaemia:
606   A review. *African Vision and Eye Health* 77:7. 10.4102/aveh.v77i1.439
607   Mattugini N, Merl-Pham J, Petrozziello E, Schindler L, Bernhagen J, Hauck SM, and Gotz M.
608   2018. Influence of white matter injury on gray matter reactive gliosis upon stab wound in
609   the adult murine cerebral cortex. *Glia* 66:1644-1662. 10.1002/glia.23329
610   Mazade RE, and Eggers ED. 2020. Inhibitory components of retinal bipolar cell receptive fields
611   are differentially modulated by dopamine D1 receptors. *Visual Neuroscience* 37:E01.
612   10.1017/S0952523819000129
613   McDowell RE, Barabas P, Augustine J, Chevallier O, McCarron P, Chen M, McGeown JG, and
614   Curtis TM. 2018. Muller glial dysfunction during diabetic retinopathy in rats is reduced by
615   the acrolein-scavenging drug, 2-hydrazino-4,6-dimethylpyrimidine. *Diabetologia*
616   61:2654-2667. 10.1007/s00125-018-4707-y

617 Menduni F, Davies LN, Madrid-Costa D, Fratini A, and Wolffsohn JS. 2018. Characterisation of
618 the porcine eyeball as an in-vitro model for dry eye. *Contact Lens and Anterior Eye*
619 41:13-17. 10.1016/j.clae.2017.09.003
620 Mesquida M, Drawnel F, and Fauser S. 2019. The role of inflammation in diabetic eye disease.
621 *Seminars in Immunopathology* 41:427-445. 10.1007/s00281-019-00750-7
622 Mi XS, Yuan TF, Ding Y, Zhong JX, and So KF. 2014. Choosing preclinical study models of
623 diabetic retinopathy: key problems for consideration. *Drug Design, Development and*
624 *Therapy* 8:2311-2319. 10.2147/DDDT.S72797
625 Ogurtsova K, da Rocha Fernandes JD, Huang Y, Linnenkamp U, Guariguata L, Cho NH, Cavan
626 D, Shaw JE, and Makaroff LE. 2017. IDF Diabetes Atlas: Global estimates for the
627 prevalence of diabetes for 2015 and 2040. *Diabetes Research and Clinical Practice*
628 128:40-50. 10.1016/j.diabres.2017.03.024
629 Ola MS, Berkich DA, Xu Y, King MT, Gardner TW, Simpson I, and LaNoue KF. 2006. Analysis
630 of glucose metabolism in diabetic rat retinas. *Am J Physiol Endocrinol Metab*
631 290:E1057-1067. 10.1152/ajpendo.00323.2005
632 Poitry-Yamate C, and Tsacopoulos M. 1991. Glial (Muller) cells take up and phosphorylate
633 [3H]2-deoxy-D-glucose in mammalian retina. *Neurosci Lett* 122:241-244. 10.1016/0304-
634 3940(91)90868-t
635 Ponsioen TL, van Luyn MJ, van der Worp RJ, Pas HH, Hooymans JM, and Los LI. 2008.
636 Human retinal Muller cells synthesize collagens of the vitreous and vitreoretinal interface
637 in vitro. *Molecular Vision* 14:652-660.
638 Renner S, Blutke A, Clauss S, Deeg CA, Kemter E, Merkus D, Wanke R, and Wolf E. 2020.
639 Porcine models for studying complications and organ crosstalk in diabetes mellitus. *Cell*
640 *and Tissue Research* 380:341-378. 10.1007/s00441-019-03158-9
641 Renner S, Braun-Reichhart C, Blutke A, Herbach N, Emrich D, Streckel E, Wunsch A, Kessler
642 B, Kurome M, Bahr A, Klymiuk N, Krebs S, Puk O, Nagashima H, Graw J, Blum H,
643 Wanke R, and Wolf E. 2013. Permanent neonatal diabetes in INS(C94Y) transgenic
644 pigs. *Diabetes* 62:1505-1511. 10.2337/db12-1065
645 Robel S, Mori T, Zoubaa S, Schlegel J, Sirko S, Faissner A, Goebbels S, Dimou L, and Gotz M.
646 2009. Conditional deletion of beta1-integrin in astroglia causes partial reactive gliosis.
647 *Glia* 57:1630-1647. 10.1002/glia.20876
648 Ruzafa N, Pereiro X, Aspichueta P, Araiz J, and Vecino E. 2018a. The Retina of Osteopontin
649 deficient Mice in Aging. *Mol Neurobiol* 55:213-221. 10.1007/s12035-017-0734-9
650 Ruzafa N, Pereiro X, Lepper MF, Hauck SM, and Vecino E. 2018b. A Proteomics Approach to
651 Identify Candidate Proteins Secreted by Muller Glia that Protect Ganglion Cells in the
652 Retina. *PROTEOMICS* 18:e1700321. 10.1002/pmic.201700321
653 Saeedi P, Petersohn I, Salpea P, Malanda B, Karuranga S, Unwin N, Colagiuri S, Guariguata L,
654 Motala AA, Ogurtsova K, Shaw JE, Bright D, Williams R, and Committee IDFDA. 2019.
655 Global and regional diabetes prevalence estimates for 2019 and projections for 2030
656 and 2045: Results from the International Diabetes Federation Diabetes Atlas, 9(th)
657 edition. *Diabetes Res Clin Pract* 157:107843. 10.1016/j.diabres.2019.107843
658 Schnichels S, Kiebler T, Hurst J, Maliha AM, Loscher M, Dick HB, Bartz-Schmidt KU, and
659 Joachim SC. 2019. Retinal Organ Cultures as Alternative Research Models. *Altern Lab*
660 *Anim* 47:19-29. 10.1177/0261192919840092
661 Sorrentino FS, Allkabes M, Salsini G, Bonifazzi C, and Perri P. 2016. The importance of glial
662 cells in the homeostasis of the retinal microenvironment and their pivotal role in the
663 course of diabetic retinopathy. *Life Sci* 162:54-59. 10.1016/j.lfs.2016.08.001
664 Subirada PV, Paz MC, Ridano ME, Lorenc VE, Vaglienti MV, Barcelona PF, Luna JD, and
665 Sanchez MC. 2018. A journey into the retina: Muller glia commanding survival and
666 death. *Eur J Neurosci* 47:1429-1443. 10.1111/ejn.13965

667 Syrbe S, Kuhrt H, Gartner U, Habermann G, Wiedemann P, Bringmann A, and Reichenbach A.
668   2018. Muller glial cells of the primate foveola: An electron microscopical study.
669   *Experimental eye research* 167:110-117. 10.1016/j.exer.2017.12.004
670 Szklarczyk D, Gable AL, Lyon D, Junge A, Wyder S, Huerta-Cepas J, Simonovic M, Doncheva
671   NT, Morris JH, Bork P, Jensen LJ, and Mering CV. 2019. STRING v11: protein-protein
672   association networks with increased coverage, supporting functional discovery in
673   genome-wide experimental datasets. *Nucleic Acids Res* 47:D607-D613.
674   10.1093/nar/gky1131
675 Taylor L, Arner K, Taylor IH, and Ghosh F. 2014. Feet on the ground: Physical support of the
676   inner retina is a strong determinant for cell survival and structural preservation in vitro.
677   *Invest Ophthalmol Vis Sci* 55:2200-2213. 10.1167/iovs.13-13535
678 Thomas RL, Halim S, Gurudas S, Sivaprasad S, and Owens DR. 2019. IDF Diabetes Atlas: A
679   review of studies utilising retinal photography on the global prevalence of diabetes
680   related retinopathy between 2015 and 2018. *Diabetes Research and Clinical Practice*
681   157. 10.1016/j.diabres.2019.107840
682 Toft-Kehler AK, Skytt DM, Svare A, Lefevere E, Van Hove I, Moons L, Waagepetersen HS, and
683   Kolko M. 2017. Mitochondrial function in Müller cells - Does it matter? *Mitochondrion*
684   36:43-51. https://doi.org/10.1016/j.mito.2017.02.002
685 Umpierrez G, and Korytkowski M. 2016. Diabetic emergencies — ketoacidosis, hyperglycaemic
686   hyperosmolar state and hypoglycaemia. *Nature Reviews Endocrinology* 12:222-232.
687   10.1038/nrendo.2016.15
688 Valdes J, Trachsel-Moncho L, Sahaboglu A, Trifunovic D, Miranda M, Ueffing M, Paquet-
689   Durand F, and Schmachtenberg O. 2016. Organotypic retinal explant cultures as in vitro
690   alternative for diabetic retinopathy studies. *ALTEX* 33:459-464. 10.14573/altex.1603111
691 Vujosevic S, Micera A, Bini S, Berton M, Esposito G, and Midena E. 2015. Aqueous Humor
692   Biomarkers of Muller Cell Activation in Diabetic Eyes. *Invest Ophthalmol Vis Sci*
693   56:3913-3918. 10.1167/iovs.15-16554
694 Wahl V, Vogler S, Grosche A, Pannicke T, Ueffing M, Wiedemann P, Reichenbach A, Hauck
695   SM, and Bringmann A. 2013. Osteopontin inhibits osmotic swelling of retinal glial
696   (Muller) cells by inducing release of VEGF. *Neuroscience* 246:59-72.
697   10.1016/j.neuroscience.2013.04.045
698 Weigand M, Degroote RL, Amann B, Renner S, Wolf E, Hauck SM, and Deeg CA. 2020.
699   Proteome profile of neutrophils from a transgenic diabetic pig model shows distinct
700   changes. *J Proteomics* 224.
701 Wisniewski JR, Zougman A, Nagaraj N, and Mann M. 2009. Universal sample preparation
702   method for proteome analysis. *Nat Methods* 6:359-362. 10.1038/nmeth.1322
703 Yang J, Chen C, McLaughlin T, Wang Y, Le Y-Z, Wang JJ, and Zhang SX. 2019. Loss of X-box
704   binding protein 1 in Müller cells augments retinal inflammation in a mouse model of
705   diabetes. *Diabetologia* 62:531-543. 10.1007/s00125-018-4776-y
706 Yokomizo H, Maeda Y, Park K, Clermont AC, Hernandez SL, Fickweiler W, Li Q, Wang CH,
707   Paniagua SM, Simao F, Ishikado A, Sun B, Wu IH, Katagiri S, Pober DM, Tinsley LJ,
708   Avery RL, Feener EP, Kern TS, Keenan HA, Aiello LP, Sun JK, and King GL. 2019.
709   Retinol binding protein 3 is increased in the retina of patients with diabetes resistant to
710   diabetic retinopathy. *Sci Transl Med* 11. 10.1126/scitranslmed.aau6627
711 Yu H, Liu X, and Zhong Y. 2017. The Effect of Osteopontin on Microglia. *Biomed Res Int*
712   2017:1879437. 10.1155/2017/1879437
713 Yu T, Sheu S-S, Robotham JL, and Yoon Y. 2008. Mitochondrial fission mediates high glucose-
714   induced cell death through elevated production of reactive oxygen species.
715   *Cardiovascular research* 79:341-351. 10.1093/cvr/cvn104

716 Yu Y, Li W, Wojciechow B, Jenkins AJ, and Lyons TJ. 2007. Effects of D- and L-Glucose and
717   Mannitol on Retinal Capillary Cells: Inhibition by Nanomolar Aminoguanidine. *American*
718   *Journal of Pharmacology and Toxicology* 2:148-158. 10.3844/ajptsp.2007.148.158
719 Zhang D, Fei Q, Li J, Zhang C, Sun Y, Zhu C, Wang F, and Sun Y. 2016. 2-Deoxyglucose
720   Reverses the Promoting Effect of Insulin on Colorectal Cancer Cells In Vitro. *PLoS One*
721   11:e0151115. 10.1371/journal.pone.0151115
722 Zhang JZ, Gao L, Widness M, Xi X, and Kern TS. 2003. Captopril inhibits glucose accumulation
723   in retinal cells in diabetes. *Investigative Ophthalmology & Visual Science* 44:4001-4005.
724   10.1167/iovs.02-1193
725 Zhu ZX, Cai WH, Wang T, Ye HB, Zhu YT, Chi LS, Duan YM, Sun CC, Xuan YH, and Jin LT.
726   2015. bFGF-Regulating MAPKs Are Involved in High Glucose-Mediated ROS Production
727   and Delay of Vascular Endothelial Cell Migration. *PLoS One* 10:e0144495-e0144495.
728   10.1371/journal.pone.0144495
729
730

Figure 1

Retinal RMG proteome profiling in a diabetic cell culture model system

Experimental workflow: Primary retinal RMG were isolated from eyes of adult pigs. After 14 days in vitro, cells were treated in three different conditions for 72 hours. After treatments, cells were lysed and proteolysed proteins quantified by label-free LC-MS/MS-based proteomic analysis applying a data-independent acquisition mode.
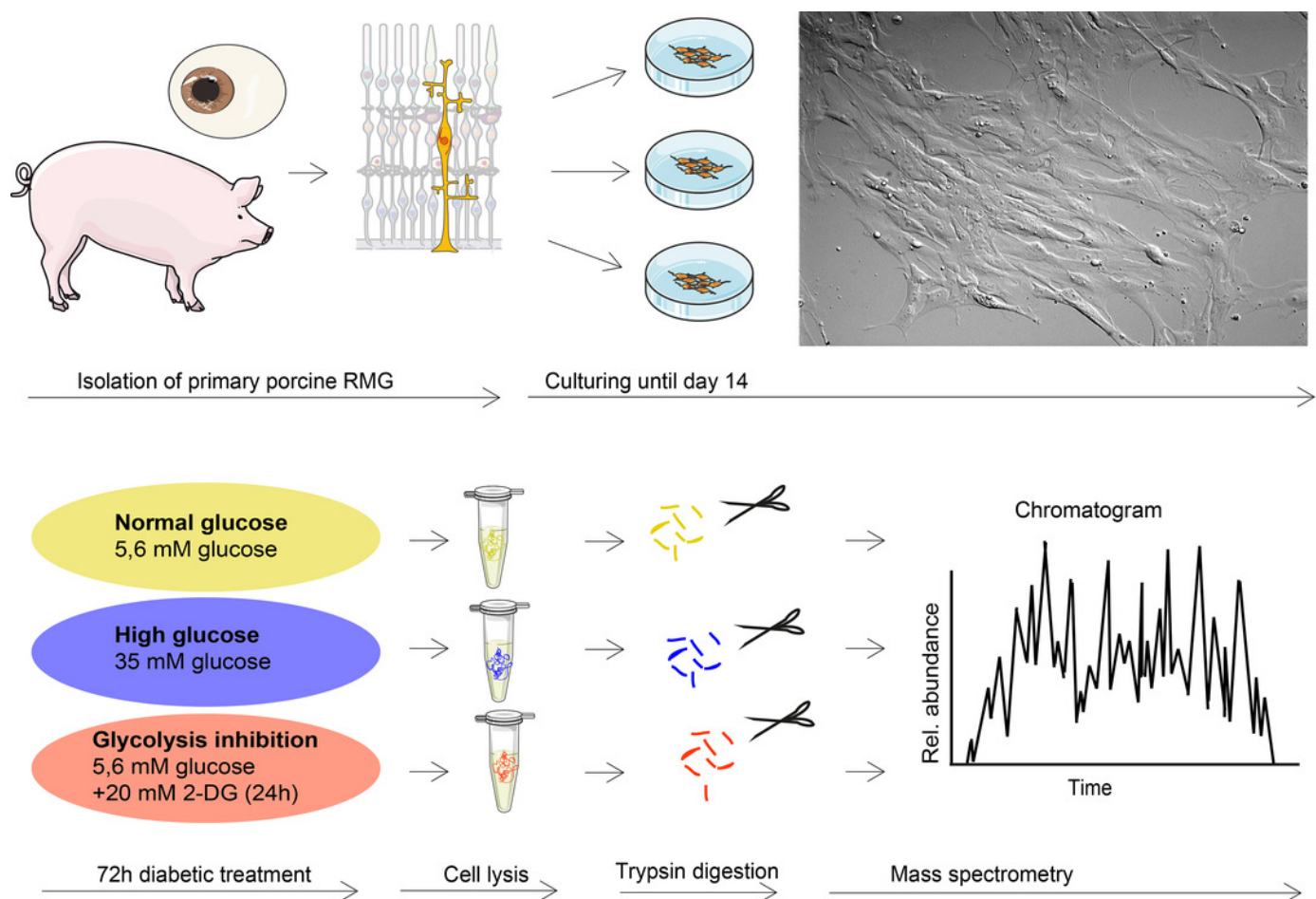
Figure 2

Differential protein abundances from primary porcine RMG in high glucose (a,b) or glycolysis inhibition (c,d) treatment compared to normoglycemic treatment group

Volcano plots illustrating the log2 transformed abundance fold change of quantified proteins (? 2 unique peptides) between the high glucose (a) or glycolysis inhibition (b) and normoglycemic group plotted against the corresponding negative log10 transformed p-value. Reference lines illustrate a p-value of 0.05 and a 1.33-fold or 0.75-fold differential abundance level. Significantly (p-value < 0.05) changed proteins with ? 1.33 (blue/red) or ? 0.75-fold (yellow) differential expression levels are colored. ECM-related proteins are labeled by gene names. (b), (d) Top ten most significantly altered biological processes in hyperglycemic (b) or glycolysis inhibition (d) treatment group according to Genomatix Gene Ranker Database. The three highest ranking processes in each condition belong to the context of ECM.
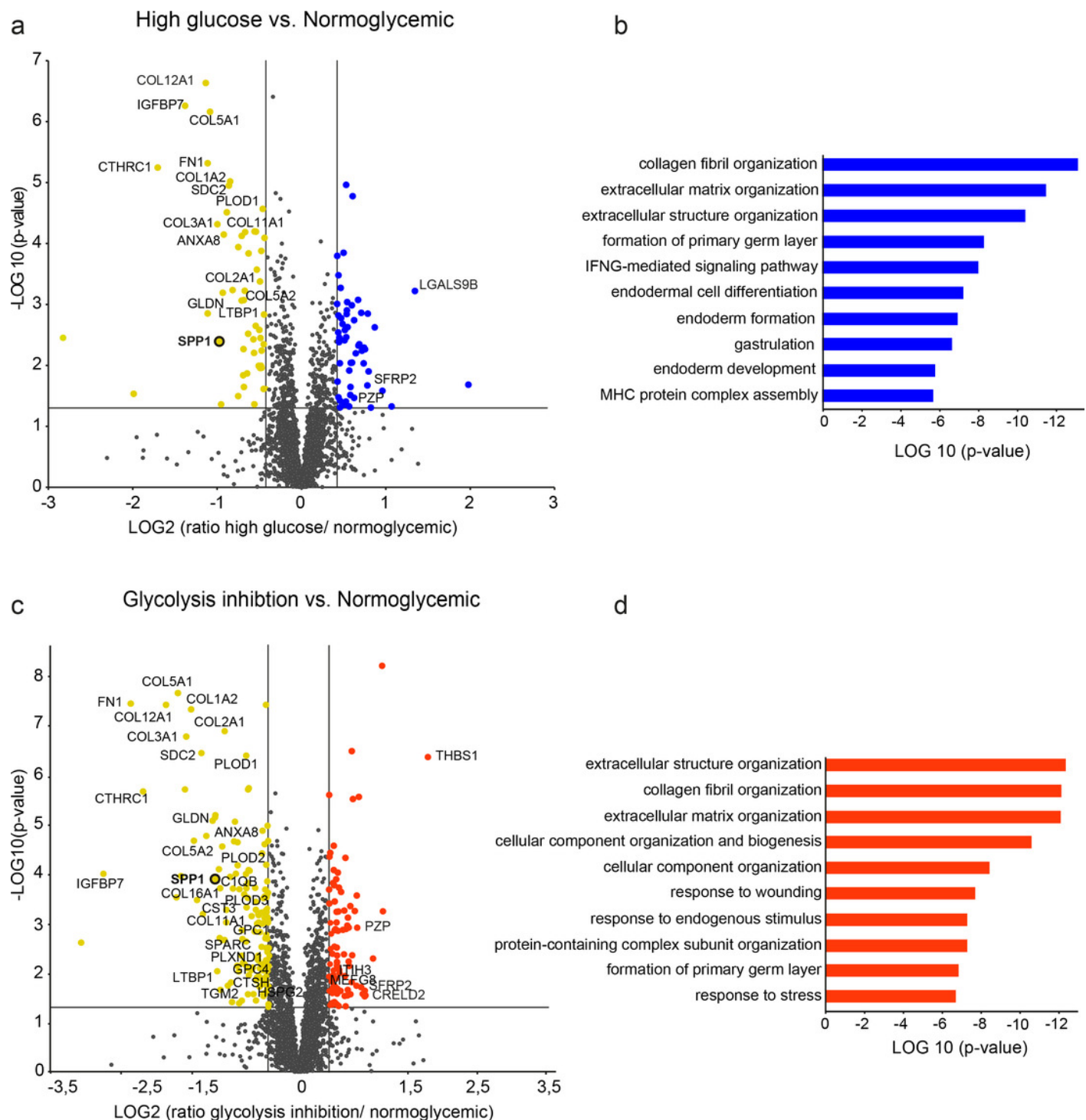
Figure 3

Overlap of proteins from primary porcine RMG with differential abundance in high glucose and glycolysis inhibition compared to normoglycemic treatment group points to affected ECM organization and cellular adhesions

Overlap of proteins with differential abundance in high glucose and glycolysis inhibition compared to normoglycemic treatment group points to affected ECM organization and cellular adhesions (a) Venn diagram of all proteins with differential abundance (criteria: ≥ 2 unique peptides, p-value < 0.05, fold change ≥ 1.33 or ≤ 0.75-fold) in hyperglycemic (blue) and glycolysis inhibition (red) compared to normoglycemic treatment group. (b) STRING protein functional association network of 65 overlapping proteins that display differential abundance in hyperglycemic and glycolysis inhibition compared to normoglycemic treatment group. Colored protein symbols belong to the GO term biological process "ECM organization" (yellow) and "cellular adhesion" (red).
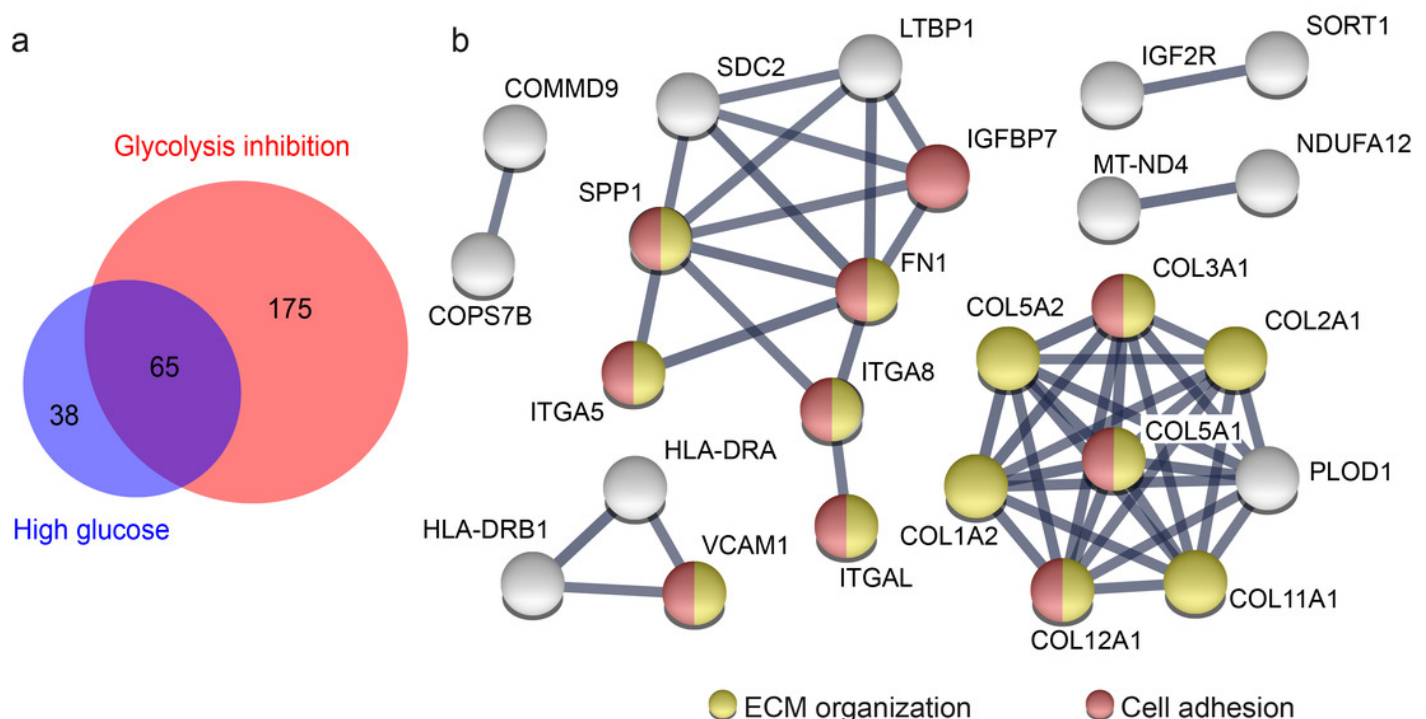
Figure 4

Validation in a porcine diabetic retinal explant culture model

(a) Left: Nasal pole of a left pig eye, recognizable by the slight bulge of the eyeball (arrow). At the temporal pole, the corneal limbus tapers (asterisk). The optic nerve on the back of the eyeball is located slightly below the horizontal center and slightly temporal. Right: The same eye opened. A horizontal band extending from the nasal to the temporal pole nearby the optic disk (illustrated by ><) is called "visual streak" and is distinguished by high densities of cones and ganglion cells (Garca et al. 2005; Hendrickson & Hicks 2002). Explants were excised from this region dorso-nasal of the optic disc (circle). (b) Explants were cultured at the fluid/air interface on polycarbonate membrane with one drop of medium on the top. Treatments were performed for three days.

a
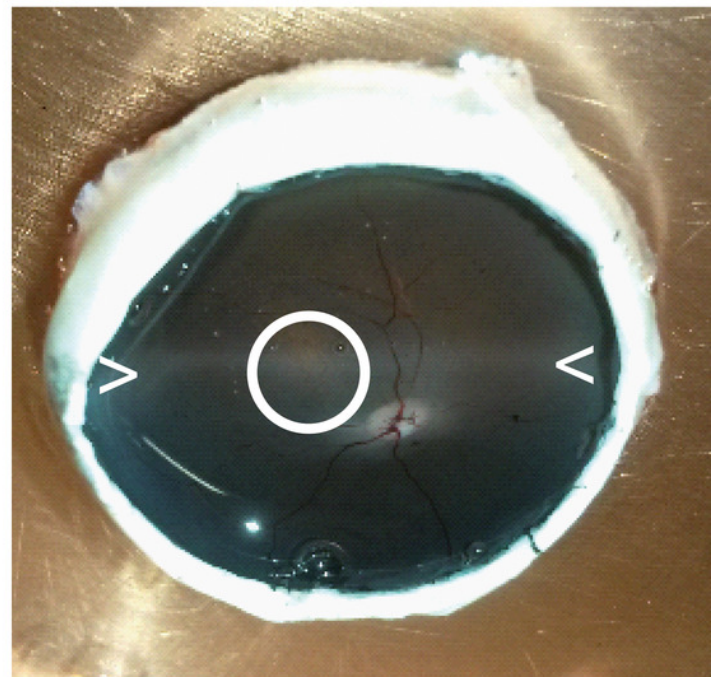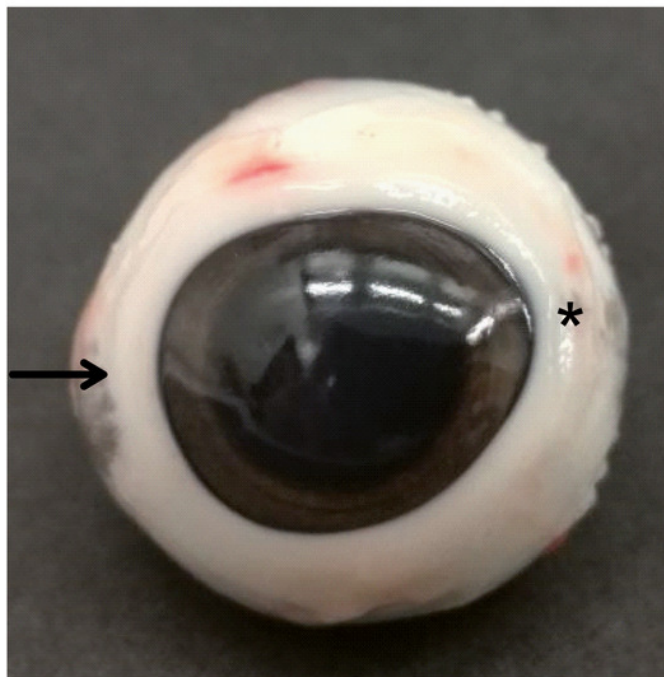
Selection and preparation of porcine retinal explants

b
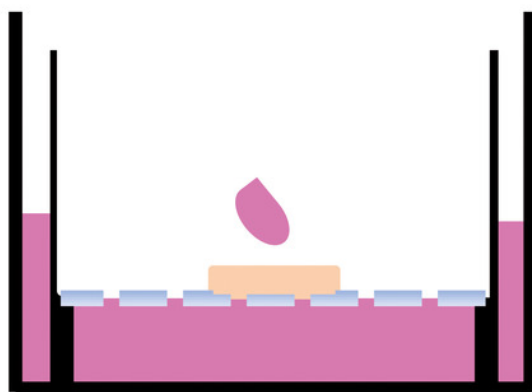
72h diabetic treatment

Figure 5

Immunohistochemical verification of SPP1 abundances in retinal organotypic explants upon different treatment conditions

Retinal expression of SPP1 (left panel, green) and vimentin (mid panel, red) in representative explants cultured under normoglycemic (n=4), osmotic control (n=4), high glucose (n=4) and glycolysis inhibition (n=4) conditions for 72 hours. SPP1 was expressed at the level of POS independently of the culture condition. Expression along the inner neuroretina in the normoglycemic condition was associated with RMG, as demonstrated by the overlay image of SPP1 and vimentin stainings (top, right panel, yellow), but diminished in all other conditions. Nuclei are stained with HOECHST in blue. GCL, ganglion cell layer, NFL, nerve fiber layer, IPL, inner plexiform layer, INL, inner nuclear layer, OPL, outer plexiform layer, ONL, outer nuclear layer, POS, photoreceptor outer segments